

TECHNICAL RESEARCH REPORT

Decentralized Control of Autonomous Vehicles

by John S. Baras, Xiaobo Tan, Pedram Hovareshti

CSHCN TR 2003-8
(ISR TR 2003-14)



The Center for Satellite and Hybrid Communication Networks is a NASA-sponsored Commercial Space Center also supported by the Department of Defense (DOD), industry, the State of Maryland, the University of Maryland and the Institute for Systems Research. This document is a technical report in the CSHCN series originating at the University of Maryland.

Web site <http://www.isr.umd.edu/CSHCN/>

Report Documentation Page				Form Approved OMB No. 0704-0188	
Public reporting burden for the collection of information is estimated to average 1 hour per response, including the time for reviewing instructions, searching existing data sources, gathering and maintaining the data needed, and completing and reviewing the collection of information. Send comments regarding this burden estimate or any other aspect of this collection of information, including suggestions for reducing this burden, to Washington Headquarters Services, Directorate for Information Operations and Reports, 1215 Jefferson Davis Highway, Suite 1204, Arlington VA 22202-4302. Respondents should be aware that notwithstanding any other provision of law, no person shall be subject to a penalty for failing to comply with a collection of information if it does not display a currently valid OMB control number.					
1. REPORT DATE 2003		2. REPORT TYPE		3. DATES COVERED -	
4. TITLE AND SUBTITLE Decentralized Control of Autonomous Vehicles				5a. CONTRACT NUMBER	
				5b. GRANT NUMBER	
				5c. PROGRAM ELEMENT NUMBER	
6. AUTHOR(S)				5d. PROJECT NUMBER	
				5e. TASK NUMBER	
				5f. WORK UNIT NUMBER	
7. PERFORMING ORGANIZATION NAME(S) AND ADDRESS(ES) Army Research Office,PO Box 12211,Research Triangle Park,NC,27709				8. PERFORMING ORGANIZATION REPORT NUMBER	
9. SPONSORING/MONITORING AGENCY NAME(S) AND ADDRESS(ES)				10. SPONSOR/MONITOR'S ACRONYM(S)	
				11. SPONSOR/MONITOR'S REPORT NUMBER(S)	
12. DISTRIBUTION/AVAILABILITY STATEMENT Approved for public release; distribution unlimited					
13. SUPPLEMENTARY NOTES The original document contains color images.					
14. ABSTRACT see report					
15. SUBJECT TERMS					
16. SECURITY CLASSIFICATION OF:			17. LIMITATION OF ABSTRACT	18. NUMBER OF PAGES 15	19a. NAME OF RESPONSIBLE PERSON
a. REPORT unclassified	b. ABSTRACT unclassified	c. THIS PAGE unclassified			

Decentralized Control of Autonomous Vehicles*

John S. Baras, Xiaobo Tan, and Pedram Hovareshti

Institute for Systems Research and

Department of Electrical and Computer Engineering

University of Maryland, College Park, MD 20742 USA

{baras, xbtan, hovaresp}@glue.umd.edu

Abstract

Decentralized control methods are appealing in coordination of multiple vehicles due to their low demand for long-range communication and their robustness to single-point failures. An important approach in decentralized multi-vehicle control involves artificial potentials or digital pheromones. In this paper we explore a decentralized approach to path generation for a group of combat vehicles in a battlefield scenario. The mission is to maneuver the vehicles to cover a target area. The vehicles are required to maintain good overall area coverage, and avoid obstacles and threats during the maneuvering. The gradient descent method is used, where each vehicle makes its moving decision by minimizing a potential function that encodes information about its neighbours, obstacles, threats and the target. We conduct analysis of vehicle behaviors by studying the vector field induced by the potential function. Simulation has shown that this approach leads to interesting emergent behaviors, and the behaviors can be varied by adjusting the weighting coefficients of different potential function terms.

1 Introduction

Autonomous unmanned vehicles (AUVs) are receiving tremendous interest due to their potentially revolutionizing applications in defense, transportation, weather forecast, and planetary exploration [1]. These vehicles are often deployed in groups to perform complicated missions. Communication is often limited in these applications due to the large number of vehicles involved, limited battery power, and constraints imposed by environmental conditions or mission requirements. Hence a decentralized approach to co-

*This research was supported by the Army Research Office under the ODDR&E MURI01 Program Grant No. DAAD19-01-1-0465 to the Center for Networked Communicating Control Systems (through Boston University).

ordination and control of multi-vehicles is especially appealing. A decentralized method has another advantage over a centralized one: it is more robust to the problem of single-point failure.

Inspired by the emergent behaviors demonstrated by swarms of bacteria, insects, and animals, control methods which yield desired collective behaviors based on simple local interactions are of great interest [2, 3, 4]. Artificial potentials or digital pheromones are typically involved in such methods for multi-vehicle control, see e.g., [3, 5, 6, 4] and the references therein. The potential function method has been used in various robotic applications [7]. The idea is to derive a force or other input (e.g., velocity) from some potential function which encodes relevant information about the environment and the mission.

In this paper we explore a decentralized approach to path generation for a group of combat vehicles in a battlefield scenario using the potential function method. The mission is to maneuver the vehicles to cover a target area. The vehicles are also expected to maintain good overall area coverage during the maneuvering, and avoid obstacles and threats. At every time instant each vehicle evaluates its potential function profile and decides its velocity based on the gradient descent method. The potential function consists of several terms reflecting the objectives and the constraints. It is constructed in such a way that only information about neighbouring vehicles, local information about dynamic threats, and some static information (about stationary threats, targets) are involved.

We analyze vehicle formations at equilibria by taking the sum of potential functions of all vehicles as a Lyapunov function candidate. We also study the behavior of a vehicle experiencing both attraction from the target and repulsion from the obstacles by analyzing its vector field. Simulation is performed in Matlab, and it shows that the decentralized approach leads to interesting emergent behaviors, and the behaviors can be varied by adjusting the weighting coefficients of different potential function terms.

The remainder of the paper is organized as follows. In Section 2 we describe the problem setup and construct the potential functions. We perform analysis of vehicle behaviors in Section 3. Simulation results are reported in Section 4. Section 5 concludes the paper.

2 Potential Functions

We study the kinematic planning problem for N vehicles moving on a (two dimensional) plane. Extension to three dimensional space is straightforward, although the analysis will be more complicated. Each vehicle is treated as a point. The coordinates of the i -th vehicle V_i is denoted as $p_i = (x_i, y_i)$, $1 \leq i \leq N$.

The task for the vehicles is to move toward and then occupy a connected target area $A \subset \mathbb{R}^2$. They should avoid to crash into obstacles that are distributed in the battlefield. There are also threats, both

stationary ones and moving ones, that endanger the vehicles if they are close. We assume that each vehicle has the knowledge of locations of stationary threats, and it can detect a moving threat if the threat is within the distance R_m .

The vehicles can talk to each other and exchange information about their positions and velocities if they are within the neighbouring distance R_c . Let $\mathcal{V}(t)$ be the set of vehicles alive at t . For $V_i \in \mathcal{V}(t)$, we define its neighbouring set

$$\mathcal{N}(V_i) \triangleq \{V_j \in \mathcal{V}(t) : \|p_i - p_j\| \leq R_c\}.$$

If two or more vehicles get too close, there is a chance of collision. That also makes it easier for the enemy fire to target the vehicles. Another disadvantage of being too close is that the overall coverage area is small. On the other hand, if vehicles are too far apart, they lose contact. Therefore, there is an optimal distance $r_0 < R_c$ between two vehicles.

From the above discussions, there are multiple objectives/constraints when a vehicle makes the moving decision. To accomodate that we construct a potential function \bar{J}_t^i for each vehicle V_i at time t , where \bar{J}_t^i consists of several terms, each term reflecting a goal or a constraint. To be specific,

$$\bar{J}_t^i = \lambda_g J^g(p_i(t)) + \lambda_n J^n(p_i(t), \{p_j(t)\}_{j \neq i}) + \lambda_o J^o(p_i(t)) + \lambda_s J^s(p_i(t)) + \lambda_m J^m(p_i(t), t), \quad (1)$$

where J^g, J^n, J^o, J^s, J^m are components of the potential function relating to the target, neighbouring vehicles, obstacles, stationary threats, and moving threats, respectively, and $\lambda_g, \lambda_n, \lambda_o, \lambda_s$, and $\lambda_m \geq 0$ are weighting coefficients. The velocity of the vehicle V_i is specified by

$$\dot{p}_i(t) = -\frac{\partial \bar{J}_t^i}{\partial p_i}. \quad (2)$$

We now describe in detail the components of the potential function.

- The target potential J^g . Denote $\rho(p, A) = \inf_{a \in A} \|p - a\|$, the distance from the point p to the target area A . We then let

$$J^g(p_i) = f^g(\rho(p_i, A)),$$

where $f^g(\cdot)$ is a strictly increasing function, and $f^g(0) = 0$. This guarantees that in the absence of other objects, the vehicle will move toward the target. For analysis and simulation in this paper, we choose $f^g(r) = r^2$.

- The neighbouring potential J^n . Since distance (as opposed to direction) is our concern here, we let

$$J^n(p_i(t), \{p_j(t)\}_{j \neq i}) = \sum_{j \neq i: V_j \in \mathcal{N}(V_i)} f^n(\|p_i(t) - p_j(t)\|), \quad (3)$$

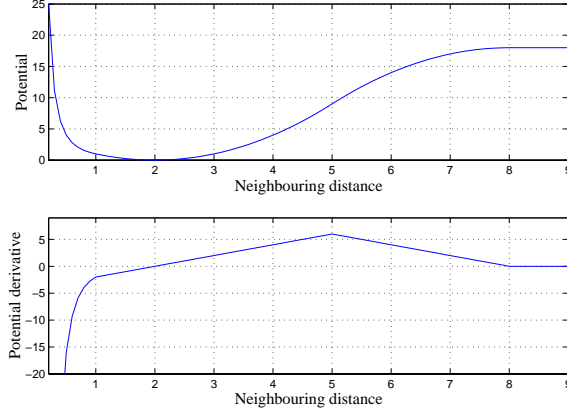


Figure 1: An example of the neighbouring potential function.

where $f^n : \mathbb{R}^+ \rightarrow \mathbb{R}$ is a differentiable function that has the following properties: a) $f^n(r)$ approaches infinity as $r \rightarrow 0$, and is strictly decreasing in $[0, r_0]$; b) it is strictly increasing in $[r_0, R_c]$ and $\frac{df^n}{dr}(R_c) = 0$. These properties enable two vehicles to keep the optimal distance in the absence of other objects, and make the dynamics transition seamless when the neighbouring set of a vehicle is changing. An example of such f^n and its derivative is shown in Figure 1, where $r_0 = 2$, $R_c = 8$.

- The obstacle potential J^o . An obstacle is a connected, closed set (could be a single point) that a vehicle cannot enter. We assume that there are a finite number of obstacles $\{O_j\}_{j=1}^{N_o}$. Then

$$J^o(p_i) = \sum_{j=1}^{N_o} f^o(\rho(p_i, O_j)), \quad (4)$$

where $\rho(p_i, O_j)$ is the distance from p_i to the set O_j , and $f^o(\cdot) : \mathbb{R}^+ \rightarrow \mathbb{R}$ is a strictly decreasing function and $f^o(r) \rightarrow \infty$ as $r \rightarrow 0$. One example of f^o is $f^o(r) = \frac{1}{r^2}$.

- The potential J^s due to stationary threats. Stationary threats can be modeled similarly as obstacles, so that vehicles will avoid to get close to them. Anisotropic threats (dangers that are direction-dependent) can be taken care of using appropriate potential functions.
- The potential J^m due to moving threats. A moving threat is a moving point mass. The i -th vehicle is able to see the moving threat M_j if $\|p_i - q_j\| \leq R_d$, and is killed by M_j if $\|p_i - q_j\| \leq R_e < R_d$, where q_j denotes the position of M_j . Let $\mathcal{M}_i(t)$ be the set of moving threats in the i -th vehicle's detection range, then we let

$$J^m(p_i, t) = \sum_{j: M_j \in \mathcal{M}_i(t)} f^m(\|p_i - q_j\|), \quad (5)$$

where the function $f^m : (R_e, \infty) \rightarrow \mathbb{R}$ is differentiable, strictly decreasing on (R_e, R_d) , constant on (R_d, ∞) , and $f^m(r) \rightarrow \infty$ when $r \rightarrow R_e$. One can see that with this potential function, a vehicle

tries to keep at least a distance R_e from moving threats, and its vector field remains continuous when moving threats enter or leave its detection range. A simple example for such $f^m(\cdot)$ is

$$f^m(r) = \begin{cases} \frac{1}{(r-R_e)^2} & \text{if } R_e < r \leq \frac{R_e+R_d}{2} \\ \frac{16(r-R_d)^2}{(R_d-R_e)^3(R_d+R_e)} - \frac{8R_e}{(R_d-R_e)^3} & \text{if } \frac{R_e+R_d}{2} \leq r \leq R_d \\ -\frac{8R_e}{(R_d-R_e)^3} & \text{if } r > R_d \end{cases}$$

3 Qualitative Analysis of Vehicle Behaviors

In this section, we analyze vehicle behaviors under the gradient descent method. In particular, we analyze how vehicles settle down after they enter the target area, and study the behavior of a vehicle when it experiences both attraction from the target and the repulsion from the obstacles.

3.1 Stability of equilibrium configurations

We first consider multi-vehicles inside the target area. We are interested in knowing whether the vehicles will settle down for an equilibrium configuration under interactions, and if so, whether the equilibrium configuration is stable. Here we assume that the only component of the potential function of each vehicle is J^n .

Proposition 3.1 *Let N be the number of vehicles.*

1. *For any N , the configuration of vehicles converges to an equilibrium under interactions.*
2. *For $N = 2$, the vehicles maintain a distance of r_0 in the equilibrium configuration and the equilibrium is globally stable.*
3. *For $N = 3$, assuming that $\frac{df^n}{dr}$ is strictly increasing in $(0, r_0]$, there are two possible equilibrium configurations, equilateral triangular with spacing r_0 (Figure 2 (a)), and collinear with equal spacing r' (Figure 2 (b)), where $\frac{r_0}{2} < r' < r_0$ and*

$$\frac{df^n}{dr}(r') = -\frac{df^n}{dr}(2r'). \quad (6)$$

If $\frac{df^n}{dr}$ is strictly increasing in $[r_0, 2r_0]$, r' is unique. The collinear configuration is unstable, while the equilateral configuration is stable.

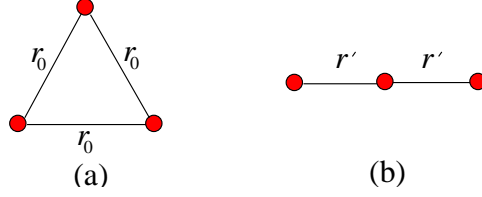


Figure 2: Equilibrium configurations for $N = 3$.

Proof. 1. Define a candidate Lyapunov function

$$J(\{p_i(t)\}) = \frac{1}{2} \sum_{i=1}^N J^n(p_i(t), \{p_j(t)\}_{j \neq i}).$$

It's easy to verify that

$$\frac{dJ}{dt} = - \sum_{i=1}^N \left\| \frac{\partial J^n}{\partial p_i}(p_i, \{p_j\}_{j \neq i}) \right\|^2. \quad (7)$$

Hence J is nonincreasing with t . Since J is lower bounded, $\frac{dJ}{dt} \rightarrow 0$. This implies that $\dot{p}_i(t) \rightarrow 0$, $\forall i$, and hence the vehicles converge to an equilibrium configuration.

2. When $N = 2$, $J(p_1(t), p_2(t)) = f^n(\|p_1(t) - p_2(t)\|)$. Writing $r_{12}(t) = \|p_1(t) - p_2(t)\|$, we have

$$\frac{dJ}{dt} = -2 \left(\frac{df^n}{dr}(r_{12}(t)) \right)^2.$$

Hence $r_{12}(t) \rightarrow r_0$ as $t \rightarrow \infty$, and it's clear that this is a stable configuration (as long as $\|p_1(0) - p_2(0)\| < R_c$).

3. When $N = 3$,

$$J(p_1(t), p_2(t), p_3(t)) = f^n(r_{12}(t)) + f^n(r_{23}(t)) + f^n(r_{31}(t)),$$

where $r_{ij}(t) = \|p_i(t) - p_j(t)\|$. Then $\frac{dJ}{dt} =$

$$- \left\| \frac{df^n}{dr}(r_{12}) \hat{\mathbf{r}}_{12} + \frac{df^n}{dr}(r_{31}) \hat{\mathbf{r}}_{13} \right\|^2 - \left\| \frac{df^n}{dr}(r_{12}) \hat{\mathbf{r}}_{21} + \frac{df^n}{dr}(r_{23}) \hat{\mathbf{r}}_{23} \right\|^2 - \left\| \frac{df^n}{dr}(r_{31}) \hat{\mathbf{r}}_{31} + \frac{df^n}{dr}(r_{23}) \hat{\mathbf{r}}_{32} \right\|^2, \quad (8)$$

where $\hat{\mathbf{r}}_{ij}$ denotes the unit vector pointing from p_j to p_i . Eq. (8) implies J is strictly decreasing unless either

- $\frac{df^n}{dr}(r_{12}) = \frac{df^n}{dr}(r_{23}) = \frac{df^n}{dr}(r_{31}) = 0$, which corresponds to the equilateral triangular configuration shown in Figure 2 (a), or
- $\hat{\mathbf{r}}_{ij}$'s are parallel or antiparallel and, assuming p_2 is between p_1 and p_3 (we do not lose generality since three vehicles have symmetric roles), $r_{12} = r_{23} = r'$ for $r' \in (\frac{r_0}{2}, r_0)$ satisfying (6), which corresponds to the collinear configuration in Figure 2(b).

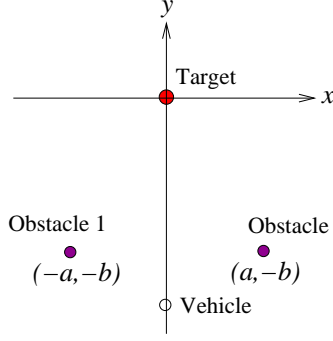


Figure 3: The setup of two obstacles and one target

The equilateral triangular configuration is stable. Indeed, for any perturbation with the corresponding $J \in (3f^n(r_0), 2f^n(r') + f^n(2r'))$, the system will come back to this configuration. The collinear configuration is not unstable, since small perpendicular perturbation of the middle vehicle leads to strict decrease of J and the system will converge to the equilateral triangular configuration.

□

Remark 3.1 *We note that similar results appeared in [6] where the second order dynamics of point masses was considered.*

3.2 Vector field analysis

First we consider the scenario as shown in Figure 3. The target is located at the origin (0,0). There are two (point) obstacles located symmetrically about the y axis with coordinates $(-a, -b)$ and $(a, -b)$, respectively, where $a, b > 0$. The potential function in terms of (x, y) is taken to be

$$\lambda_g(x^2 + y^2) + \frac{1}{(x+a)^2 + (y+b)^2} + \frac{1}{(x-a)^2 + (y+b)^2},$$

and the associated vector field is

$$\begin{cases} \dot{x}(t) = \frac{2(x+a)}{[(x+a)^2 + (y+b)^2]^2} + \frac{2(x-a)}{[(x-a)^2 + (y+b)^2]^2} - 2\lambda_g x \\ \dot{y}(t) = \frac{2(y+b)}{[(x+a)^2 + (y+b)^2]^2} + \frac{2(y+b)}{[(x-a)^2 + (y+b)^2]^2} - 2\lambda_g y \end{cases} \quad (9)$$

We consider a vehicle on the x axis, and study whether it will move toward the target under the vector field (9) when $y < 0$ (the case $y > 0$ is simpler and can be studied similarly). Due to the symmetry, $\dot{x} = 0$, so the real question is whether $\dot{y} > 0$. When $x = 0$,

$$\dot{y} = \frac{4(y+b)}{[(a^2 + (y+b)^2)^2]} - 2\lambda_g y. \quad (10)$$

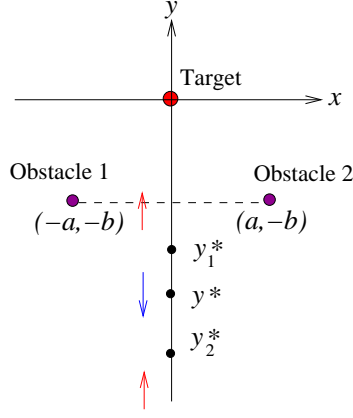


Figure 4: Vector field on the x -axis for the case of two obstacles and one target.

Let $\tilde{y} = y + b$. Obviously, if $\tilde{y} \geq 0$, $\dot{y} > 0$. In the following we study the case $\tilde{y} < 0$, i.e., $y < -b$.

Proposition 3.2 *There is a unique solution $\tilde{y}^* \in (-\frac{a}{\sqrt{3}}, 0)$ to*

$$4\tilde{y}^3 - 3b\tilde{y}^2 + a^2b = 0. \quad (11)$$

Let

$$\lambda_g^* = \frac{2}{(a^2 + \tilde{y}^{*2})^2} \left(1 - \frac{4\tilde{y}^{*2}}{a^2 + \tilde{y}^{*2}}\right).$$

Let $y^* = \tilde{y}^* - b$. Then

- If $\lambda_g > \lambda^*$, $\dot{y} > 0$, $\forall y < -b$;
- If $\lambda_g = \lambda^*$, $\dot{y} > 0$ for $y \in (-\infty, -b)$ except at y^* where $\dot{y} = 0$;
- If $\lambda_g < \lambda^*$, there exist y_1^*, y_2^* such that $y_2^* < y^* < y_1^*$, and

$$\begin{cases} \dot{y} > 0, & \text{if } y \in (-\infty, y_2^*) \\ \dot{y} < 0, & \text{if } y \in (y_2^*, y_1^*) \\ \dot{y} > 0, & \text{if } y \in (y_1^*, -b) \\ \dot{y} = 0, & \text{if } y = y_1^* \text{ or } y_2^* \end{cases},$$

as illustrated in Figure 4. Furthermore, y_1^* (y_2^* , resp.) increases (decreases, resp.) with λ and $y_1^* \rightarrow -b$, $y_2^* \rightarrow -\infty$ as $\lambda \rightarrow \infty$.

Proof. Let

$$h(\tilde{y}) = \frac{4\tilde{y}}{(a^2 + \tilde{y}^2)^2}.$$

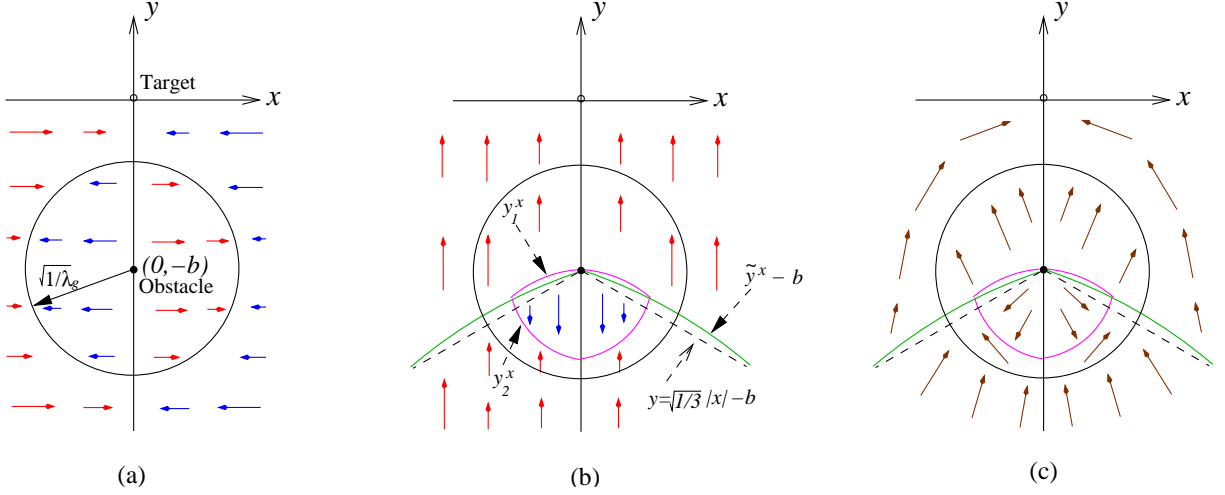


Figure 5: Vector field analysis for the case of one obstacle and one target. (a) x -component; (b) y -component; (c) total vector field.

Since

$$\frac{dh}{d\tilde{y}} = \frac{4(a^2 - 3\tilde{y}^2)}{(a^2 + \tilde{y}^2)^2}, \quad (12)$$

$h(\tilde{y})$ is strictly decreasing on $(-\infty, -\frac{a}{\sqrt{3}})$, and strictly increasing on $(-\frac{a}{\sqrt{3}}, 0)$. From (12), $\frac{dh}{d\tilde{y}}$ is also strictly increasing on $(-\frac{a}{\sqrt{3}}, 0)$. Graphical analysis reveals that there exists a unique λ_g^* , such that the line $l(\tilde{y}) = 2\lambda_g^*(\tilde{y} - b)$ is tangent to the curve $h(\tilde{y})$ at a unique $\tilde{y}^* \in (-\frac{a}{\sqrt{3}}, 0)$. After algebraic manipulations, one can show that \tilde{y}^* satisfies (11) and λ_g^* is defined by (3.2). The remaining claims of the proposition follow from the graphical analysis. \square

Next we investigate the motion of a vehicle in the presence of one target point (0,0) and one point obstacle (0, -b). Here no constraint on the vehicle position is imposed except that we focus on the region $y < 0$. The vector field is

$$\begin{cases} \dot{x} = \frac{2x}{[x^2 + (y+b)^2]^2} - 2\lambda_g x \\ \dot{y} = \frac{2(y+b)}{[x^2 + (y+b)^2]^2} - 2\lambda_g y \end{cases}. \quad (13)$$

We will discuss \dot{x} and \dot{y} separately. It's easy to show that

$$\begin{cases} \dot{x} > 0, & \text{if } (x, y) \in \{x < 0 : x^2 + (y+b)^2 > \frac{1}{\lambda_g}\} \cup \{x > 0 : x^2 + (y+b)^2 < \frac{1}{\lambda_g}\} \\ \dot{x} < 0, & \text{if } (x, y) \in \{x > 0 : x^2 + (y+b)^2 > \frac{1}{\lambda_g}\} \cup \{x < 0 : x^2 + (y+b)^2 < \frac{1}{\lambda_g}\} \\ \dot{x} = 0, & \text{if } x = 0 \text{ or } x^2 + (y+b)^2 = \frac{1}{\lambda_g} \end{cases},$$

as shown in Figure 5(a). We denote by C the circle with radius $\frac{1}{\sqrt{\lambda_g}}$ centered at (0, -b).

For \dot{y} , it's straightforward to verify

$$\dot{y} > 0 \text{ if } x^2 + (y+b)^2 > \frac{1}{\lambda_g} \text{ or } y \geq -b.$$

However, the analysis is much more involved when $y < -b$ and (x, y) is inside the circle C . The technique used in the proof of Proposition 3.2 turns out to be relevant here. Again let $\tilde{y} = y + b$. Writing

$$h_x(\tilde{y}) = \frac{2\tilde{y}}{[x^2 + \tilde{y}^2]^2},$$

for fixed x , we have

$$\frac{dh_x}{d\tilde{y}} = \frac{2(x^2 - 3\tilde{y}^2)}{(x^2 + \tilde{y}^2)^3}. \quad (14)$$

From (14), we find that $h_x(\tilde{y})$ is strictly decreasing on $(-\infty, -\frac{\sqrt{3}}{3}|x|)$ and strictly increasing on $(-\frac{\sqrt{3}}{3}|x|, 0)$ with its derivative strictly increasing on $(-\frac{\sqrt{3}}{3}|x|, 0)$. Hence there exists a unique λ_g^x , such that the line $l(\tilde{y}) = 2\lambda_g^x(\tilde{y} - b)$ is tangent to the curve $h_x(\tilde{y})$ at a unique $\tilde{y}^x \in (-\frac{\sqrt{3}}{3}|x|, 0)$. It's easy to verify that \tilde{y}^x is a solution to

$$4\tilde{y}^3 - 3b\tilde{y}^2 + bx^2 = 0, \quad (15)$$

and

$$\lambda_g^x = \frac{b^2}{16((\tilde{y}^x)^2 - b\tilde{y}^x)^3}. \quad (16)$$

Lemma 3.1 *Both \tilde{y}^x and λ_g^x strictly decrease as $|x|$ increases.*

Proof. By the implicit function theorem, \tilde{y}^x is a differentiable function of x^2 . Differentiating (15) with respect to $z = x^2$ leads to

$$\frac{d\tilde{y}^x}{dz} = \frac{-b}{12(\tilde{y}^x)^2 + 6b\tilde{y}^x} < 0,$$

since $\tilde{y}^x < 0$. From (16), λ_g^x also strictly decreases as $|x|$ increases. \square

From Lemma 3.1, for fixed $\lambda_g > 0$, there exists $\hat{x}_\lambda > 0$, such that

$$\begin{cases} \lambda_g^x = \lambda_g & \text{if } |x| = \hat{x}_\lambda \\ \lambda_g^x > \lambda_g & \text{if } |x| < \hat{x}_\lambda \\ \lambda_g^x < \lambda_g & \text{if } |x| > \hat{x}_\lambda \end{cases}.$$

Similarly as in Proposition 3.2, we have

- if $\lambda_g > \lambda_g^x$ (i.e., $|x| > \hat{x}_\lambda$), $\dot{y} > 0$, $\forall y < -b$;
- if $\lambda_g = \lambda_g^x$ (i.e., $|x| = \hat{x}_\lambda$), $\dot{y} > 0$, $\forall y \in (-\infty, -b)$ except at $y^\lambda = \tilde{y}^{\hat{x}_\lambda} - b$ where $\dot{y} = 0$;
- if $\lambda_g < \lambda_g^x$ (i.e., $|x| < \hat{x}_\lambda$), there exist y_1^x and y_2^x such that $y_2^x < \tilde{y}^x - b < y_1^x$, and

$$\begin{cases} \dot{y} > 0, & \text{if } y \in (-\infty, y_2^x) \\ \dot{y} < 0, & \text{if } y \in (y_2^x, y_1^x) \\ \dot{y} > 0, & \text{if } y \in (y_1^x, -b) \\ \dot{y} = 0, & \text{if } y = y_1^x \text{ or } y_2^x \end{cases}.$$

Lemma 3.2 $\hat{x}_\lambda^2 + (\tilde{y}^{\hat{x}_\lambda})^2 < \frac{1}{\lambda_g}$. When $|x| < \hat{x}_\lambda$, y_1^x (y_2^x , resp.) increases (decreases, resp.) as $|x|$ decreases, $\lim_{|x| \rightarrow 0} y_1^x = -b$, and $y_2^0 + b > -\frac{1}{\sqrt{\lambda_g}}$.

Proof. As is easy to verify, $\dot{y} > 0$ at (x, y) if $x^2 + (y + b)^2 > \frac{1}{\lambda_g}$. Since $\dot{y} = 0$ at $(\hat{x}_\lambda, \tilde{y}^{\hat{x}_\lambda})$, the first claim of the lemma holds.

Since for any $\tilde{y} < 0$, $h_{x_1}(\tilde{y}) > h_{x_2}(\tilde{y})$ if $|x_1| > |x_2|$, graphical analysis reveals that y_1^x (y_2^x , resp.) increases (decreases, resp.) as $|x|$ decreases, and $\lim_{|x| \rightarrow 0} y_1^x = -b$. Again, since $\dot{y} > 0$ at (x, y) if $x^2 + (y + b)^2 > \frac{1}{\lambda_g}$, the point $(0, y_2^0)$ is inside the circle C , i.e., $y_2^0 + b > -\frac{1}{\sqrt{\lambda_g}}$. \square

Figure 5 (b) and (c) sketch the y -component of the vector field and the total vector field, respectively. We can see that the only point where $\dot{x} = \dot{y} = 0$ is $(0, y_2^0)$. But this is an unstable equilibrium as one can tell from Figure 5(c). We can also verify that the linearized system at $(0, y_2^0)$ has a positive eigenvalue.

4 Simulation Results

In this section we present some results of simulation performed in Matlab. As shown in Figure 6(a), we have ten vehicles (the dots), two obstacles (the solid circles), one target (the dashed circle), and one moving threat (represented by the cross). The moving threat is assumed to move around the target with a constant angular velocity ω . We don't assume any stationary threats in the simulation. The velocity magnitude is bounded by 1. The Matlab function "fconmin" is called to solve the constrained optimization problem for each vehicle at every time instant.

Figure 6 and Figure 7 show snapshots of the trajectories of the vehicles. The weighting constants used in Figure 6 are $\lambda_g = 50$, $\lambda_n = 5$, $\lambda_o = 10^5$, $\lambda_m = 10^4$. The angular velocity of the moving threat is $\omega = 10$. We observe that due to the relatively high weight on obstacles, the vehicles take long paths to avoid vehicles; however, if we change λ_o to 10^4 , they take the shorter path passing the "potential valley" between two obstacles (Figure 7).

Figure 8 shows the effects of λ_m . When $\lambda_m = 10^4$, vehicles can successfully enter the target area (Figure 8 (a)), while they fail to do so when $\lambda_m = 10^5$ (Figure 8 (b)).

From the simulation results, we see that the decentralized approach based on potential functions lead to some emergent behaviors of vehicles. In addition, we can modify the behaviors by appropriately changing the weighting constants.

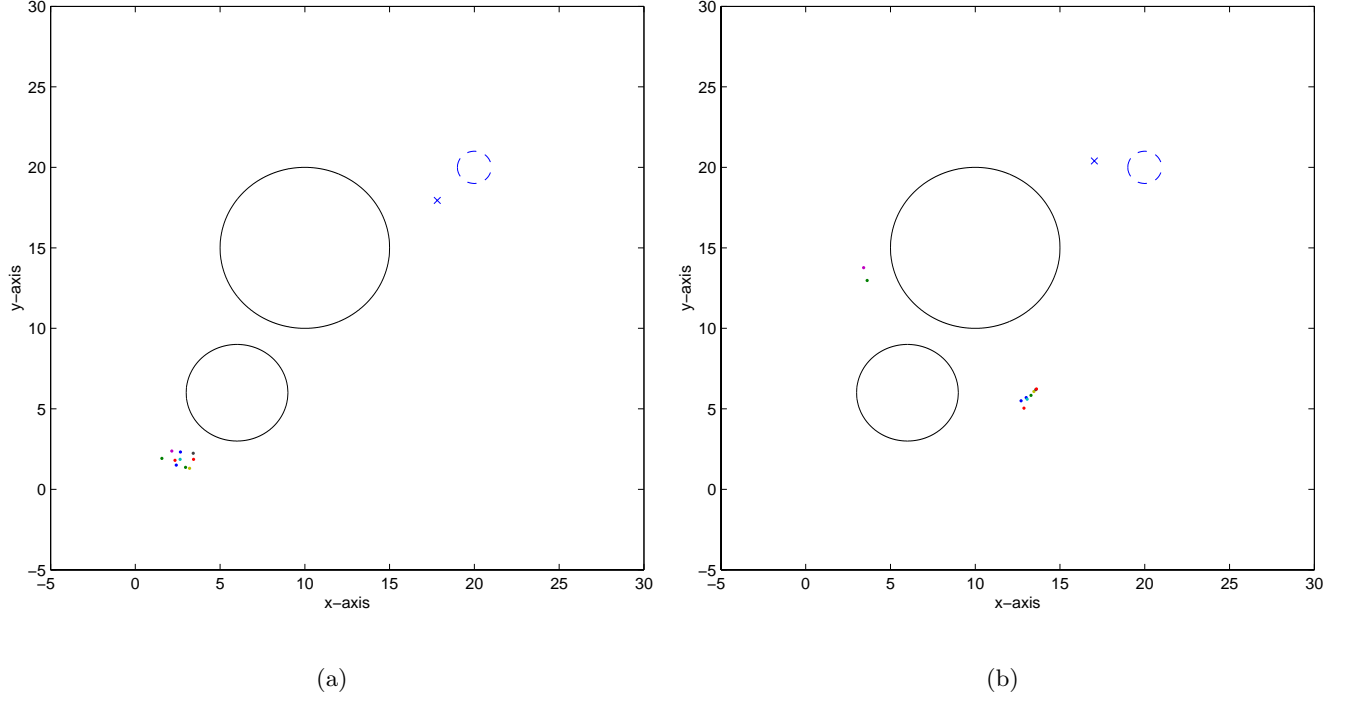


Figure 6: Snapshots for the case $\lambda_o = 10^5$: (a) Initial positions; (b) Vehicles detouring to avoid obstacles.

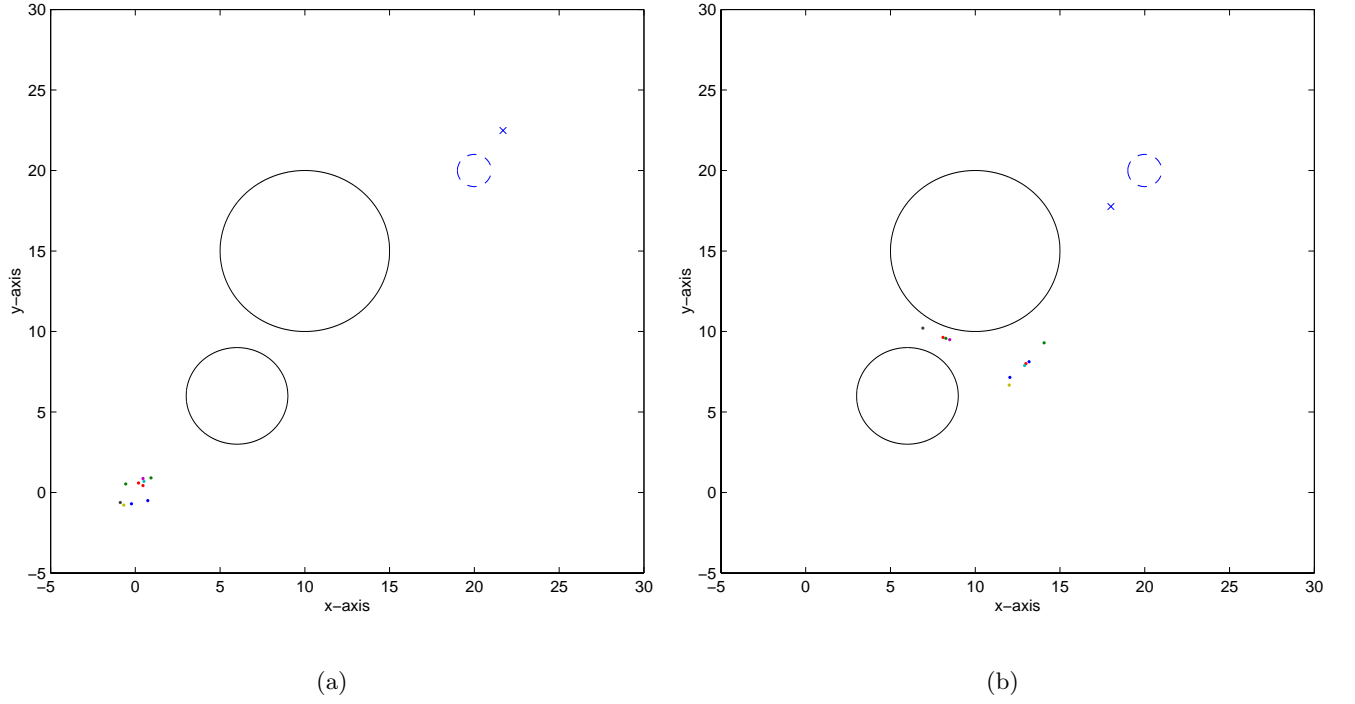


Figure 7: Snapshots for the case $\lambda_o = 10^4$: (a) Initial positions; (b) Vehicles passing the “potential valley” between obstacles.

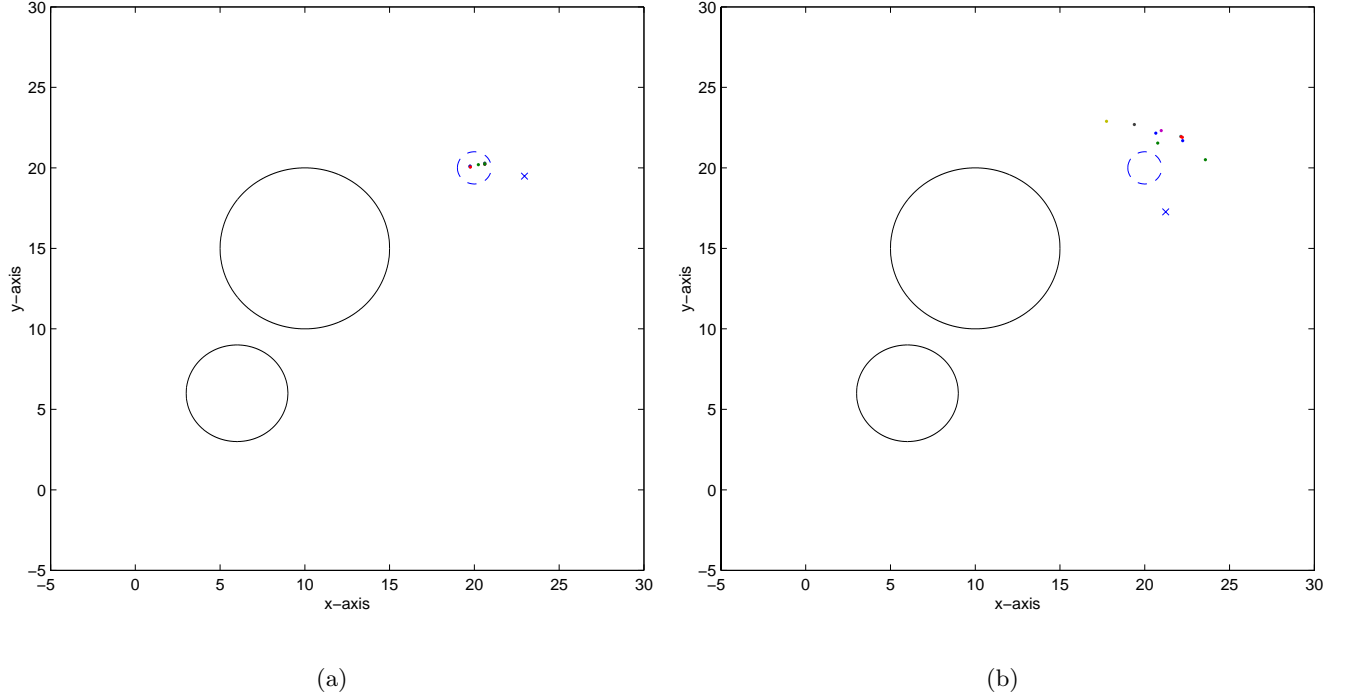


Figure 8: Effect of the parameter λ_m : (a) $\lambda_m = 10^4$ (vehicles enter the target area); (b) $\lambda_m = 10^5$ (vehicles fail to enter the target area).

5 Conclusions

In this paper we have developed a decentralized approach to coordination and control of multi-vehicles using potential functions. We designed potential function terms for different objectives or constraints. A battlefield mission scenario was considered, where the vehicles were required to occupy a target area (or point), avoid obstacles, evade threats, and maintain reasonable inter-vehicle distances. Preliminary analysis of vehicle behaviors was presented. Simulation was conducted and interesting emergent behaviors were observed.

The most important advantage of this approach is simplicity since only local and static information is needed in the path generation. It is also flexible and robust, which is of vital importance in complex, dynamic environments such as the battlefields. The disadvantage is that the possibility of being trapped in local minima exists, which has been a long time concern in the studies of the potential function method [8]. Practically interactions between vehicles and dynamic changes in the environment may prevent a vehicle from being trapped. Artificially introduced perturbation will also help to resolve this problem [9].

Ongoing work includes analysis of vehicle behaviors in the presence of vehicle interactions as well as

attractions/repulsions from other objects.

References

- [1] D. A. Schoenwald, “AUVs: in space, air, water, and on the ground,” *IEEE Control Systems Magazine*, vol. 20, no. 6, pp. 15–18, Dec. 2000.
- [2] K. M. Passino, “Biomimicry of bacterial foraging for distributed optimization and control,” *IEEE Control Systems Magazine*, vol. 22, no. 3, pp. 52–67, 2002.
- [3] N. E. Leonard and E. Fiorelli, “Virtual leaders, artificial potentials and coordinated control of groups,” in *Proceedings of the 40th IEEE Conference on Decision and Control*, Orlando, FL, 2001, pp. 2968–2973.
- [4] H. V. Parunak, M. Purcell, and R. O’Connel, “Digital pheromones for autonomous coordination of swarming UAV’s,” in *Proceedings of AIAA 1st Technical Conference and Workshop on Unmanned Aerospace Vehicles, Systems, and Operations*, 2002.
- [5] R. Olfati-Saber and R. M. Murray, “Distributed cooperative control of multiple vehicle formations using structural potential functions,” in *Proceedings of the 15th IFAC World Congress*, Barcelona, Spain, 2002.
- [6] R. Bachmayer and N. E. Leonard, “Vehicle networks for gradient descent in a sampled environment,” in *Proceedings of the 41st IEEE Conference on Decision and Control*, Las Vegas, NV, 2002, pp. 112–117.
- [7] E. Rimon and D. E. Koditschek, “Exact robot navigation using artificial potential functions,” *IEEE Transactions on Robotics and Automation*, vol. 8, no. 5, pp. 501–518, 1992.
- [8] R. Volpe and P. Khosla, “Manipulator control with superquadric artificial potential functions: theory and experiments,” *IEEE Transactions on Systems, Man, and Cybernetics*, vol. 20, no. 6, pp. 1423–1436, 1990.
- [9] J. Barraquand, L. Kavraki, J. Latombe, T. Li, R. Motwani, and P. Raghavan, “A random sampling scheme for path planning,” *International Journal of Robotics Research*, vol. 16, no. 6, pp. 759–774, 1997.